



# Prospects of CKM elements $|V_{cs}|$ and decay constant $f_{D_s^+}$ in $D_s^+ \rightarrow \mu^+ \nu_\mu$ decay at STCF

Jia-Jun Liu<sup>1</sup>, Xiao-Dong Shi<sup>2,3</sup> , Hui-Jing Li<sup>4,5</sup>, Xiao-Rong Zhou<sup>2,3,a</sup> , Bo Zheng<sup>1,b</sup>

<sup>1</sup> University of South China, Hengyang 421000, People's Republic of China

<sup>2</sup> State Key Laboratory of Particle Detection and Electronics, Hefei 230026, People's Republic of China

<sup>3</sup> School of Physical Sciences, University of Science and Technology of China, Hefei 230026, People's Republic of China

<sup>4</sup> Henan Normal University, Xinxiang 453007, People's Republic of China

<sup>5</sup> National Demonstration Center for Experimental Physics Education, Henan Normal University, Xinxiang 453007, China

Received: 1 October 2021 / Accepted: 25 March 2022 / Published online: 19 April 2022

© The Author(s) 2022

**Abstract** We report a feasibility study of pure leptonic decay  $D_s^+ \rightarrow \mu^+ \nu_\mu$  by using a fast simulation software package at STCF. With an expected luminosity of  $1 \text{ ab}^{-1}$  collected at STCF at a center-of-mass energy of 4.009 GeV, the statistical sensitivity of the branching fraction is determined to be 0.3%. Combining this result with the  $c \rightarrow s$  quark mixing matrix element  $|V_{cs}|$  determined from the current global Standard Model fit, the statistical sensitivity of  $D_s^+$  decay constant,  $f_{D_s^+}$ , is estimated to be 0.2%. Alternatively, combining the current results of  $f_{D_s^+}$  calculated by lattice QCD, the statistical sensitivity of  $|V_{cs}|$  is determined to be 0.2%, which helps probe possible new physics beyond Standard Model. The unprecedented precision to be achieved at STCF will provide a precise calibration of QCD and rigorous test of Standard Model.

## 1 Introduction

The proposed Super Tau-Charm Facility (STCF) [1] in China is a symmetric electron-positron collider that will provide  $e^+e^-$  annihilation at center-of-mass (c.m.) energies  $\sqrt{s}$  ranging from 2.0 to 7.0 GeV. The peak luminosity is expected to be  $0.5 \times 10^{35} \text{ cm}^{-2} \text{ s}^{-1}$  or higher at  $\sqrt{s} = 4.0 \text{ GeV}$  and it will accumulate an integrated luminosity ( $\mathcal{L}$ ) of more than  $1 \text{ ab}^{-1}$  per year. By operating at  $\sqrt{s} = 4.009 \text{ GeV}$ , the STCF will produce  $2.0 \times 10^8 D_s^+ D_s^-$  with one-year's data collection, enabling researchers to study the purely leptonic, semileptonic and hadronic decays of  $D_s^+$  with unprecedented precision.

Among these, the purely leptonic decay  $D_s^+ \rightarrow \ell^+ \nu_\ell$  ( $\ell = e, \mu$  or  $\tau$ ) provides a unique window into both strong and weak effects in the charm sector. In the Standard Model (SM), the partial width of the decay  $D_s^+ \rightarrow \ell^+ \nu_\ell$  can be written as [2]

$$\Gamma_{D_s^+ \rightarrow \ell^+ \nu_\ell} = \frac{G_F^2}{8\pi} |V_{cs}|^2 f_{D_s^+}^2 m_\ell^2 m_{D_s^+} \left(1 - \frac{m_\ell^2}{m_{D_s^+}^2}\right)^2, \quad (1)$$

where  $G_F$  is the Fermi coupling constant,  $|V_{cs}|$  is the  $c \rightarrow s$  Cabibbo-Kobayashi-Maskawa (CKM) matrix element,  $f_{D_s^+}$  is the  $D_s^+$  decay constant that parameterises the effect of the strong interaction,  $m_\ell$  and  $m_{D_s^+}$  are the masses of lepton and  $D_s^+$ , respectively. The determination of  $\Gamma_{D_s^+ \rightarrow \ell^+ \nu_\ell}$  can directly measure the product value of  $f_{D_s^+} |V_{cs}|$  because all other variables are known with high precision [3]. One can either extract  $|V_{cs}|$  by using the predicted value of  $f_{D_s^+}$  from lattice QCD (LQCD), or obtain  $f_{D_s^+}$  by using the averaged experimental value of  $|V_{cs}|$ .

Precise measurements of  $f_{D_s^+}$  [4–6] and  $|V_{cs}|$  are required to investigate new physics beyond the SM. Currently, the averaged  $f_{D_s^+}$  from various experiments indicates a  $1.5\sigma$  [7] difference from LQCD calculation [4], the latter providing a negligible uncertainty when compared to the former. Furthermore, there are  $2\sigma$  deviations for the  $|V_{cs}|$  extracted in  $D_s^+ \rightarrow l^+ \nu_l$  [7] and  $D \rightarrow Kl\nu_l$  [7], which challenges the universality for the CKM elements. The most recent  $|V_{cs}|$  and  $f_{D_s^+}$  results are still limited by the statistical uncertainty in the measurement of  $D_s^+ \rightarrow \ell^+ \nu_\ell$  [8]. More precise measurements of  $D_s^+ \rightarrow \mu^+ \nu_\mu$  are required to calibrate various theoretical calculations of  $f_{D_s^+}$  and test the unitarity of the CKM matrix.

<sup>a</sup> e-mail: zrxong@ustc.edu.cn (corresponding author)

<sup>b</sup> e-mail: zhengb@usc.edu.cn (corresponding author)

The SM predicts that the ratio of decay widths for  $D_s^+ \rightarrow \tau^+ \nu_\tau$  and  $D_s^+ \rightarrow \mu^+ \nu_\mu$  will be 9.75, with negligible uncertainty. Lepton flavour universality (LFU) could be violated with some new physics mechanisms, such as a two-Higgs-doublet model with the mediation of charged Higgs bosons [9, 10] or a Seesaw mechanism due to lepton mixing with Majorana neutrinos [11]. Based on the most recent experimental results, the ratio  $\Gamma_{D_s^+ \rightarrow \tau^+ \nu_\tau} / \Gamma_{D_s^+ \rightarrow \mu^+ \nu_\mu}$  is obtained to be  $9.98 \pm 0.52$  [3], which is consistent with the SM prediction within uncertainty. However, more precise measurements of  $D_s^+ \rightarrow \ell^+ \nu_\ell$  decays are required to test LFU and other physics mechanisms beyond the SM.

In this research, we present a feasibility study of  $D_s^+ \rightarrow \mu^+ \nu_\mu$  decay and estimate the sensitivity of various parameters at STCF [1], where  $D_s^+$  is from  $e^+ e^- \rightarrow D_s^+ D_s^-$  at  $\sqrt{s} = 4.009$  GeV with a production cross-section around 0.2 nb. Though the production cross-section of  $e^+ e^- \rightarrow D_s^+ D_s^{*-} + c.c$  is higher at  $\sqrt{s} = 4.18$  GeV, to be around 0.9 nb, the pair production of  $D_s^+ D_s^-$  without additional particles at 4.009 GeV lays into reconstruction of signals with greater purity and free of additional systematic uncertainties caused by  $\gamma$  or  $\pi^0$  reconstruction in  $D_s^{*-}$  decays.

This paper is organized as follows. In Sect. 2, the detector concept for STCF has been introduced as well as the Monte Carlo (MC) samples used for this study. Section 3 is the analysis of  $D_s^+ \rightarrow \mu^+ \nu_\mu$ . Section 4 is about optimizing of detector response, and Sect. 5 is the results and discussion.

## 2 STCF detector and MC simulation

The STCF detector under development is a general purpose detector for  $e^+ e^-$  collider. It consists of a tracking system composed of inner and outer trackers, a particle identification (PID) system with excellent  $K/\pi$  identification, an electromagnetic calorimeter (EMC) with an excellent energy resolution and a good position resolution for photons or electrons, a superconducting solenoid and a muon detector (MUD) that provides good  $\mu/\pi$  separation. The preliminary conceptual design for each sub-detector can be found in Ref. [12].

Currently, the STCF detector and the corresponding offline software system are in the research and development [13]. STCF has thus developed fast simulation software to access the physics reaches [12], which takes the most common event generator as input to perform a realistic simulation. It takes into account the effects of charged particle tracking efficiency and momentum resolution, PID efficiency, photon detection efficiency and energy/position resolution, and kinematic fits. The fast simulation also includes a pliable interface for adjusting the performance of each subsystem, which can be used to optimize the detector design based on physical constraints. The process  $D_s^+ \rightarrow \mu^+ \nu_\mu$

analysed here also serves as a benchmark process for the optimization of detector response, e.g. tracking efficiency,  $\mu/\pi$  suppression power.

A pseudo-data sample, corresponding to an integrated luminosity of  $0.1 \text{ ab}^{-1}$ , is produced at  $\sqrt{s} = 4.009$  GeV, which includes all open charm processes, initial state radiation (ISR) production of the  $\psi(3770)$ ,  $\psi(3686)$  and  $J/\psi$ , and  $q\bar{q}$  ( $q = u, d, s$ ) continuum processes, as well as Bhabha scattering,  $\mu^+ \mu^-$ ,  $\tau^+ \tau^-$  and  $\gamma\gamma$  events. The open charm processes are generated using CONEXC [14]. The effects of ISR [15] and final state radiation (FSR) [16] are considered. The decay modes with known branching fractions (BFs) are generated using EVTGEN [17] and the remaining modes are generated using LUNDCHARM [18]. The passage of particles through the detector is simulated by the fast simulation software [12].

## 3 Analysis of $D_s^+ \rightarrow \mu^+ \nu_\mu$

A double-tag technique is used to measure the absolute BF of signal process  $D_s^+ \rightarrow \mu^+ \nu_\mu$ . When a  $D_s^-$  meson (also known as the single-tag (ST)  $D_s^-$  meson) is fully reconstructed, the presence of a  $D_s^+$  meson is guaranteed. In the systems recoiling against the ST  $D_s^-$  mesons, we can select the leptonic decays of  $D_s^+ \rightarrow \mu^+ \nu_\mu$  (called the double-tag (DT) events).

In  $e^+ e^-$  collision at  $\sqrt{s} = 4.009$  GeV,  $D_s^\pm$  mesons are produced from the process  $e^+ e^- \rightarrow D_s^+ D_s^-$ . Using this threshold production characteristic, we can measure the absolute BF for  $D_s^+$  decays with a DT method. In this analysis, the ST  $D_s^-$  mesons are reconstructed from 14 hadronic decay modes,  $D_s^- \rightarrow K^+ K^- \pi^-, K^+ K^- \pi^- \pi^0, \pi^+ \pi^- \pi^-, K_S^0 K^-, K_S^0 K^- \pi^0, K^- \pi^+ \pi^-, K_S^0 K_S^0 \pi^-, K_S^0 K^+ \pi^- \pi^-, K_S^0 K^- \pi^+ \pi^-, \eta_{\gamma\gamma} \pi^-, \eta_{\pi^0 \pi^+ \pi^-} \pi^-, \eta'_{\eta_{\gamma\gamma} \pi^+ \pi^-} \pi^-, \eta'_{\gamma \rho^0} \pi^-,$  and  $\eta_{\gamma\gamma} \rho^-$ , where the subscripts of  $\eta^{(i)}$  represent the decay modes used to reconstruct  $\eta^{(i)}$ . Throughout this study, the charge conjugation is always implied.

Candidate charged tracks are selected when they pass the vertex and acceptance requirements in fast simulation.

The  $K_S^0$  candidates are reconstructed from pairs of oppositely charged tracks, which satisfy a vertex-constrained fit to a common point. The two charged tracks with minimum  $\chi^2$  of vertex fit are assumed to be pions produced by  $K_S^0$ . The  $K_S^0$  is required to have an invariant mass in range  $0.485 < M_{\pi^+ \pi^-} < 0.512 \text{ GeV}/c^2$ . In addition, the decay length of the reconstructed  $K_S^0$  must be greater than  $2\sigma$  of the vertex resolution away from the interaction point. The  $\pi^0$  and  $\eta$  mesons are reconstructed via  $\gamma\gamma$  decays. For photon candidates, they are also required to pass the criteria for neutral showers in fast simulation. The  $\gamma\gamma$  combinations with invariant masses  $M_{\gamma\gamma} \in (0.115, 0.150)$  and  $(0.500, 0.570) \text{ GeV}/c^2$  are regarded as  $\pi^0$  and  $\eta$  mesons, respectively. A kinematic

fit is performed to constrain  $M_{\gamma\gamma}$  to the  $\pi^0$  or  $\eta$  nominal mass. The  $\eta$  candidates for the  $\eta\pi^-$  ST channel are also reconstructed using  $\pi^0\pi^+\pi^-$  candidates with its invariant mass in the range (0.530, 0.570)  $\text{GeV}/c^2$ . The  $\eta'$  mesons are reconstructed via two decay modes,  $\eta\pi^+\pi^-$  and  $\gamma\rho^0$ , whose invariant masses must be between (0.946, 0.970) and (0.940, 0.976)  $\text{GeV}/c^2$ , respectively. Furthermore, the minimum energy of the  $\gamma$  from  $\eta' \rightarrow \gamma\rho^0$  decays must be greater than 0.1 GeV. The  $\rho^0$  and  $\rho^+$  mesons are reconstructed from  $\pi^+\pi^-$  and  $\pi^+\pi^0$  candidates, whose invariant masses must be greater than 0.5  $\text{GeV}/c^2$  and within (0.670, 0.870)  $\text{GeV}/c^2$ , respectively. For  $\pi^+\pi^-\pi^-$  and  $K^-\pi^+\pi^-$  tags, the dominant peaking backgrounds from  $D_s^- \rightarrow K_S^0\pi^-$  and  $D_s^- \rightarrow K_S^0K^-$  events with  $K_S^0 \rightarrow \pi^+\pi^-$  are rejected by requiring the invariant mass of any  $\pi^+\pi^-$  combination to be more than 0.03  $\text{GeV}/c^2$  away from the nominal  $K_S^0$  mass [3].

Two kinematic variables ( $\Delta E$ ,  $M_{\text{BC}}$ ) reflecting energy and momentum conservation are used to identify the tagged  $D_s^-$  candidates. First, we calculate the energy difference

$$\Delta E = E_{D_s^-} - E_{\text{beam}}, \tag{2}$$

where  $E_{D_s^-}$  is the reconstructed energy of a tagged  $D_s^-$  meson and  $E_{\text{beam}}$  is the beam energy. Correctly reconstructed signal

events peak around zero in the  $\Delta E$  distribution. To improve the signal purity, requirements of  $\Delta E$  are applied, which corresponds to  $\pm 3\sigma_{\Delta E}$  where  $\sigma_{\Delta E}$  is the resolution of  $\Delta E$  for each tag mode. If there are multiple  $D_s^-$  candidates for each tag mode, the one with minimum  $|\Delta E|$  is retained for further analysis. The second variable is the beam-energy constrained mass

$$M_{\text{BC}} = \sqrt{E_{\text{beam}}^2/c^4 - \mathbf{p}_{D_s^-}^2/c^2}, \tag{3}$$

where  $\vec{p}_{D_s^-}$  is the three-momentum of the tagged  $D_s^-$  candidate. Figure 1 shows the  $M_{\text{BC}}$  distributions for pseudo-data. The ST yields are obtained by fitting the  $M_{\text{BC}}$  distributions, where the signal is modeled using a MC-determined signal shape and the background is represented by an ARGUS [19] function. To select the signal process with a high purity, a mass window is required on  $M_{\text{BC}}$  within  $\pm 3\sigma_{M_{\text{BC}}}$ , where  $\sigma_{M_{\text{BC}}}$  is a resolution of  $M_{\text{BC}}$  determined by fitting with a double-Gaussian function.

The  $D_s^+ \rightarrow \mu^+\nu_\mu$  candidate events are selected in the recoil side of the tagged  $D_s^-$ . We require that there is only one candidate charged track in the remaining particles with the opposite charge as the tagged  $D_s^-$ . The charged track is identified as a muon candidate after passing the corre-

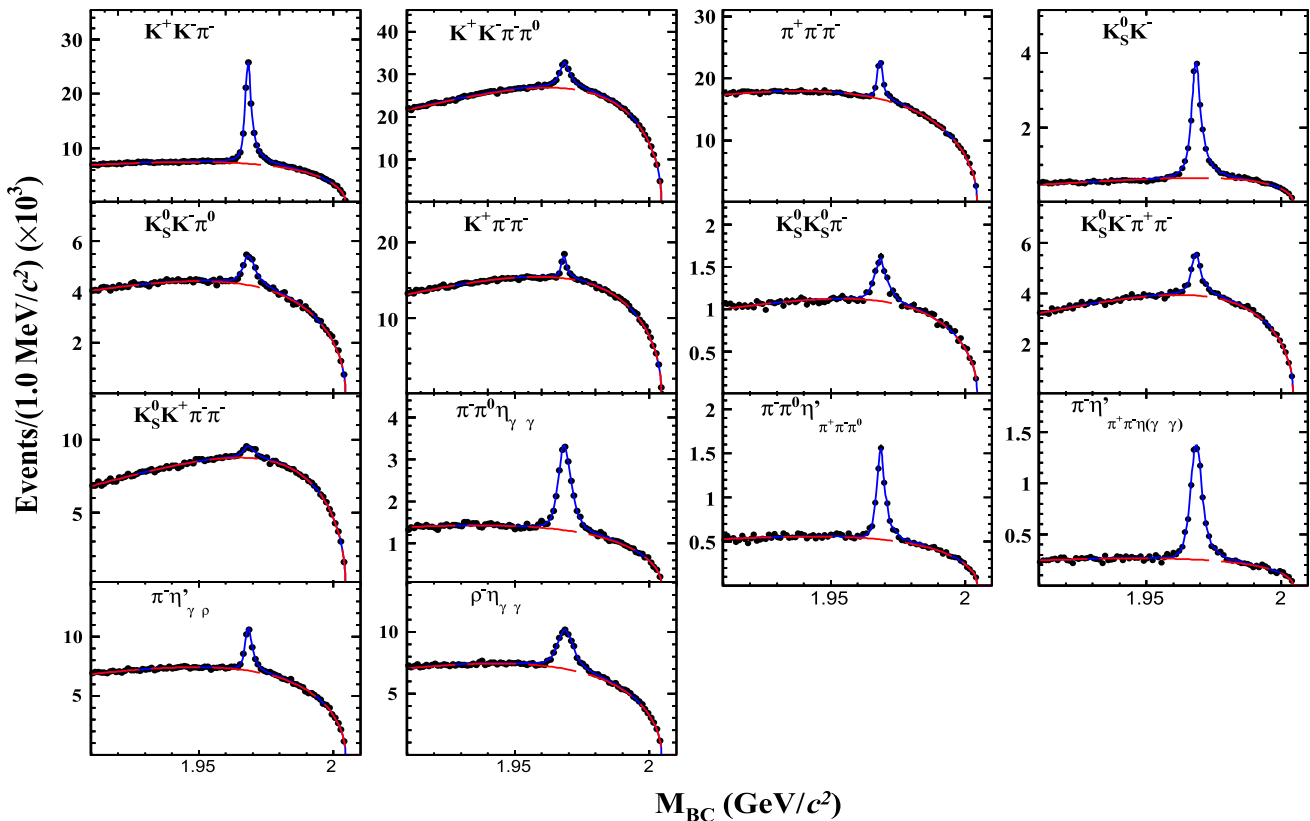


**Fig. 1** Fits to the  $M_{\text{BC}}$  distributions of  $D_s^-$  candidates, whose channels are single tag modes. The points with error bars are the pseudo-data. The blue curves are the fit results. The red curves are the fitted combinatorial backgrounds

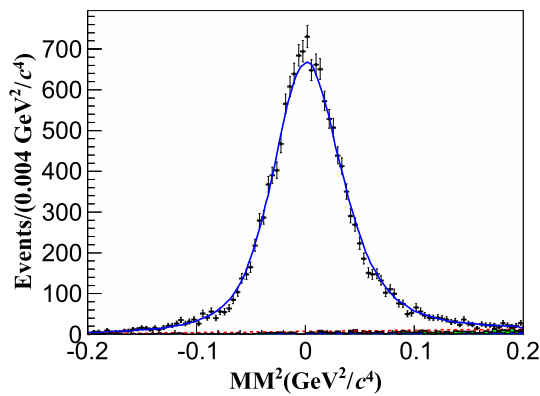


**Fig. 2** Fit to the  $MM^2$  distribution of the  $D_s^+ \rightarrow \mu^+ \nu_\mu$  candidates. Dots with error bars are the pseudo-data. Blue solid curve is the fit result. Red dotted curve is the fitted background. Green and red cross-hatched histograms are the BKG I component, and blue histogram is the BKG II component, respectively

sponding requirements in fast simulation [12]. To suppress the backgrounds with extra photon(s), the maximum energy of the unused showers ( $E_{\text{extra } \gamma}^{\text{max}}$ ) is required to be less than 0.4 GeV.

The background events that survived from the above selection criteria can be categorised into two types. The first type, noted as BKG I, contains a correctly reconstructed  $D_s^-$  but the signal side is incorrectly reconstructed from  $D_s^+ \rightarrow \tau^+ \nu_\tau$  and other  $D_s^+$  decays. The contribution of BKG I is estimated using exclusive MC samples and the fit specifies the normalised number of events. The second type noted as BKG II, contains the non- $D_s^+$  background, which is expected to be a smooth distribution under the  $D_s^-$  peak in the  $M_{\text{BC}}$  spectra. The contribution of BKG II can be estimated using  $M_{\text{BC}}$  side-band events, defined as (1.915, 1.935) GeV/ $c^2$  and (1.990, 2.000) GeV/ $c^2$ .

To characterise the signal of  $D_s^+ \rightarrow \mu^+ \nu_\mu$ , the missing mass squared ( $MM^2$ ) is used, defined as

$$MM^2 = (E_{\text{beam}} - E_{\mu^+})^2 / c^4 - \left( -\mathbf{p}_{D_s^-} - \mathbf{p}_{\mu^+} \right)^2 / c^2 \quad (4)$$

where  $E_{\mu^+}$  and  $\vec{p}_{\mu^+}$  are the energy and momentum of the muon candidate, respectively. The signal yield is extracted by fitting the combined  $MM^2$  distribution from all 14 tag modes, with a shape extracted from the signal MC sample describing the signal and a first-order Chebychev polynomial describing the background, as shown in Fig. 2.

The BF of the  $D_s^+ \rightarrow \mu^+ \nu_\mu$  is calculated by

$$\mathcal{B}_{D_s^+ \rightarrow \mu^+ \nu_\mu} = \frac{N_{\text{sig}}}{N_{\text{tag}} \times \bar{\epsilon}_{\text{sig}}}, \quad (5)$$

where  $N_{\text{sig}}$  is the number of the signal events determined by a fit to the  $MM^2$  spectrum, and  $N_{\text{tag}}$  is the number of events

for all ST modes by fits to the  $M_{\text{BC}}$ . The averaged detection efficiency for  $D_s^+ \rightarrow \mu^+ \nu_\mu$  can be expressed as

$$\bar{\epsilon}_{\text{sig}} = \sum_i \left( \frac{N_{\text{tag}}^i}{N_{\text{tag}}} \times \frac{\epsilon_{\text{tag, sig}}^i}{\epsilon_{\text{tag}}^i} \right) \quad (6)$$

where  $N_{\text{tag}}^i$  denotes the number of events for ST mode  $i$ ,  $\epsilon_{\text{tag, sig}}^i$  denotes the efficiency of detecting both the ST mode  $i$  and the pure leptonic decays, and  $\epsilon_{\text{tag}}^i$  is the efficiency of detecting the ST mode  $i$ . The efficiencies of ST modes are determined with an independent generic MC sample, and the efficiencies of DT modes are determined using the signal MC sample of  $e^+e^- \rightarrow D_s^+ D_s^-$ , where  $D_s^- \rightarrow 14$  tag modes and  $D_s^+ \rightarrow \mu^+ \nu_\mu$ .

With 0.1  $\text{ab}^{-1}$  pseudo-data, the number of ST events for  $D_s^-$  to 14 decay modes is determined to be  $N_{\text{tag}} = 3452605 \pm 6177$ , and the number of DT events for  $D_s^+ \rightarrow \mu^+ \nu_\mu$  is  $N_{\text{sig}} = 14687 \pm 142$ . The averaged efficiency of signal process is calculated to be  $\bar{\epsilon}_{\text{sig}} = (75.78 \pm 0.07)\%$  by combining 14 tag modes. The corresponding BF of  $D_s^+ \rightarrow \mu^+ \nu_\mu$  is calculated to be  $\mathcal{B}_{D_s^+ \rightarrow \mu^+ \nu_\mu} = (5.61 \pm 0.05) \times 10^{-3}$ . The uncertainties are statistical uncertainty from  $N_{\text{sig}}$ . The calculated BF agrees well with the input value. We can easily prospect the statistical sensitivity for the BF of  $D_s^+ \rightarrow \mu^+ \nu_\mu$  at STCF with 1  $\text{ab}^{-1}$  data as it is proportional to  $1/\sqrt{\mathcal{L}}$ , to be  $\mathcal{B}_{D_s^+ \rightarrow \mu^+ \nu_\mu} = (5.610 \pm 0.017) \times 10^{-3}$ , where the relative statistical uncertainty is 0.3%.

Since a full systematic study requires both experimental data and MC, we are limited in our ability to estimate every possible source. A more precise estimation of systematic uncertainty will not be feasible until the design and construction of the detector are completed. Therefore, a rough systematic uncertainty is estimated by referring to similar measurements from previous experiments [20–22].

First, there are reducible systematic uncertainties named  $\sigma_{\text{red}}$ , which can be normalized with the luminosity. The systematic uncertainty associated with the  $\mu$  tracking efficiency,  $\mu^+$  tracking, can be studied by  $e^+e^- \rightarrow \gamma \mu^+ \mu^-$  control sample in different  $\mu^+$  kinematic regions.

The tracking and PID efficiencies of  $\mu^+$  from the control sample can be used to correct the data/MC differences and estimate the corresponding systematic uncertainties. By scaling the data sample in  $e^+e^- \rightarrow \gamma \mu^+ \mu^-$  according to Ref. [20], the tracking and PID uncertainties of  $\mu^+$  selection are estimated to be 0.02% and 0.09%, respectively. The uncertainty due to statistical uncertainty of  $N_{\text{ST}}$  is 0.17%. The uncertainty of MC efficiency is due to the limited MC size, which is about 0.09% in the estimation of  $\bar{\epsilon}_{\text{sig}}$ . The systematic uncertainty associated with the requirement of maximum energy of extra  $\gamma$ ,  $E_{\text{extra } \gamma}^{\text{max}} < 0.4$  GeV, can be studied with a DT hadronic sample by considering the efficiency differences between data and MC simulation, which

is estimated to be about 0.02%. Analogously, the systematic uncertainty associated with the requirement of no additional good charged track,  $N_{\text{char}}^{\text{extra}} = 0$ , which is estimated to be about 0.05%. In the fit of  $MM^2$ , the number of background will be corrected by the difference of the misidentification rates for pion and kaon to muon, and the uncertainty of this correction factor, denoted as  $MM^2$ -fit1, is taken as the uncertainty, to be about 0.04%.

Second, there are irreducible systematic uncertainties that cannot be directly scaled based on the statistics,  $\delta_{\text{irred.}}$ . In this analysis, the only source of such uncertainty comes from the FSR effect, which is dominant by varying the amount of FSR photons in signal MC events, to be 0.40% [23].

Third, there are predictably optimized systematic uncertainties,  $\delta_{\text{pre.}}$ , which, in the future, can lead to more accurate results through detector optimization in many aspects. But the systematic uncertainties can't be estimated precisely at this time and have been therefore made a conservative estimate. On the one hand, the uncertainty in fit to the  $M_{\text{BC}}$  of ST  $D_s^-$ , denoted as  $Fit_{\text{ST}}$ , is estimated by varying fit range, bin size, background shape and signal shape for both data and MC to be about 0.35%. On the other hand, the uncertainty in the  $\Delta E$  requirement can be estimated to be 0.50% by varying the signal window.

Similarly, the uncertainty in the fit range of  $MM^2$ , denoted as  $MM^2$ -fit2 is estimated to be 0.60%. The uncertainty from BKGI in the fit of  $MM^2$ , denoted as  $MM^2$ -fit3, is estimated by varying the BF of the background sources, e.g.  $D_s^+ \rightarrow \tau^+(\mu^+ \nu_\mu \bar{\nu}_\tau) \nu_\tau$ , to be about 0.12%. The uncertainty from BKGII in the fit of  $MM^2$ , denoted as  $MM^2$ -fit4, is estimated by varying the fraction of non- $D_s^+ D_s^-$  component, to be 0.05%.

Radiative correction is due to the contribution from  $D_s^+ \rightarrow \gamma D_s^{*+} \rightarrow \gamma \mu^+ \nu_\mu$  [24], with  $D_s^{*+}$  as a virtual vector or axial-vector meson. This contribution is almost identical with our signal process for low energy radiated photons. So we have to estimate the number of events via radiation process and subtract it from the total signal events. The systematic uncertainty is estimated at 100% in present experimental measurements [25, 26], which means that the ratio of  $D_s^+ \rightarrow \gamma \mu^+ \nu_\mu$  to  $D_s^+ \rightarrow \mu^+ \nu_\mu$  is  $(1 \pm 1)\%$ . Based on the ability of the future detector to measure low-momentum particles and abundant statistics to be generated, this radiative process can be measured with a precision of better than 10%. As a consequence, the systematic uncertainty of radiative correction can be estimated to be 0.10% in future experimental and theoretical measurements.

Finally, The systematic uncertainties of the above three aspects are listed in Table 1.  $\delta_{\text{red.}}$  is calculated to be 0.21%,  $\delta_{\text{irred.}}$  is calculated to be 0.4% and  $\delta_{\text{pre.}}$  is calculated to be 0.87%. The total systematic uncertainty can be roughly estimated to be 1.0% by  $\delta_{\text{sys.}} = \sqrt{\delta_{\text{red.}}^2 + \delta_{\text{irred.}}^2 + \delta_{\text{pre.}}^2}$ .

**Table 1** Summarize of the systematic uncertainty in  $D_s^+ \rightarrow \mu^+ \nu_\mu$  with  $1 \text{ ab}^{-1}$  luminosity at  $\sqrt{s} = 4.009 \text{ GeV}$

Category	Source	Systematic uncertainty (%)
$\delta_{\text{red.}}$	$\mu$ tracking	0.02
	$\mu$ PID	0.09
	$N_{\text{ST}}$	0.17
	MC statistics	0.09
	$E_{\text{extra } \gamma}^{\text{max}} < 0.4 \text{ GeV}$	0.02
	$N_{\text{char}}^{\text{extra}} = 0$	0.05
	$MM^2$ -fit1	0.04
$\delta_{\text{irred.}}$	FSR	0.40
$\delta_{\text{pre.}}$	$Fit_{\text{ST}}$	0.35
	$\Delta E$	0.50
	$MM^2$ -fit2	0.60
	$MM^2$ -fit3	0.12
	$MM^2$ -fit4	0.05
	Radiative correction	0.10
	Sum	1.00

Apart from reconstructing  $D_s^+ \rightarrow \mu^+ \nu_\mu$  in the process of  $e^+ e^- \rightarrow D_s^+ D_s^-$  at 4.009 GeV, we also attempt to investigate the process in  $e^+ e^- \rightarrow D_s^+ D_s^{*-}$  at  $\sqrt{s} = 4.18 \text{ GeV}$ . In the selection, all  $\gamma$  or  $\pi^0$  need to be looped, which are not used to reconstruct the ST  $D_s^-$ . The  $\gamma$  or  $\pi^0$  candidates are required to satisfy the selection criteria for neutral tracks in fast simulation. If multiple  $\gamma$  or  $\pi^0$  or both  $\gamma$  and  $\pi^0$  are found, we choose the one with the minimum  $\Delta E'$  in the further analysis, which is defined as

$$\begin{aligned} \Delta E' &= E_{\text{cm}} - E_{\text{tag}} - E_{\text{miss}} - E_{\gamma/\pi^0}, \\ E_{\text{miss}} &= \sqrt{|\mathbf{p}_{\text{miss}}|^2 + M_{D_s^+}^2}, \\ \mathbf{p}_{\text{miss}} &= -\mathbf{p}_{\text{tag}} - \mathbf{p}_{\gamma/\pi^0}. \end{aligned} \tag{7}$$

In the process, the statistics is sufficient to guarantee a negligible statistics uncertainty. However, as discussed before, the dominant uncertainty comes from the detection of photon, which will be at a level of  $\mathcal{O}(0.01)$  in the current experiment [20]. It therefore demands an improved photon detection for STCF detector in future if use  $e^+ e^- \rightarrow D_s^+ D_s^{*-}$  to study the leptonic decay of  $D_s^+$ .

### 4 Optimization of detector response

A series of optimizations on detector responses have been performed in the results presented above, including the efficiency of charged particles and photons, momentum resolution of charged tracks, energy/position resolution of pho-

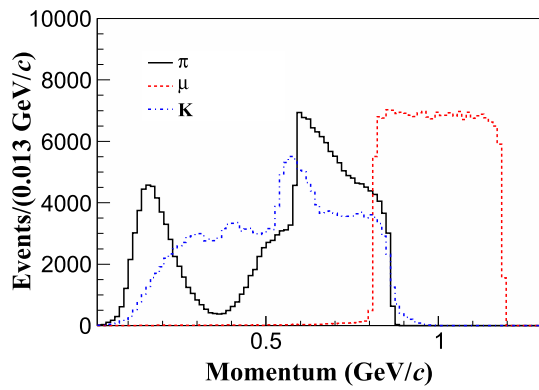


**Fig. 3** The momentum of  $\pi$ ,  $\mu$  and  $K$  from  $e^+e^- \rightarrow D_s^- D_s^+$ ,  $D_s^- \rightarrow K^+ K^- \pi^-$ ,  $D_s^+ \rightarrow \mu^+ \nu_\mu$  signal MC. The channel is generated according to the amplitude of the Dalitz plot, which describes a three-body decay process including resonances, such as  $D_s^- \rightarrow \phi(1020)\pi^- \rightarrow K^+ K^- \pi^-$ ,  $D_s^- \rightarrow f_0(980)\pi^- \rightarrow K^+ K^- \pi^-$ ,  $D_s^- \rightarrow K^*(980)^0 K^- \rightarrow K^+ K^- \pi^-$ , etc

tons, and PID efficiencies. Following that, we will go over the specifics of each of these optimizations one by one.

#### Tracking efficiency of charged tracks

The response of tracking efficiency in fast simulation is characterised by its transverse momentum  $p_T$  and polar angle  $\cos\theta$ . For high-momentum tracks, e.g.  $p_T > 0.4$  GeV/c of charged pions, the tracking efficiency within acceptance is over 99%. For low-momentum tracks, e.g.  $p_T = 0.1$  GeV/c of charged pions, the tracking efficiency is low due to various effects such as electromagnetic multiple scattering, electric field leakage, ionization energy loss etc.. Figure 3 shows the momentum distribution of charged pions in  $D_s^+$  decay, where there is a considerable number of particles with momentum lower than 0.4 GeV/c.

Benefiting from the flexible interface of changing the response of charged particles, different tracking efficiencies are set in the simulation at  $p_T$  in (0.05, 0.1) GeV/c of charged pions, where tracking efficiencies at other momenta are scaled proportionally. With an average tracking efficiency ranging from 60.16% to 90.24% for  $p_T$  in (0.05, 0.1) GeV/c, the detection efficiencies of 14 tag modes increase. The variation of detection efficiency for 14 tag modes as well as different tracking efficiencies are shown in Fig. 4a, where the optimized point is found. One can see that the ST efficiency is the most optimized with the average tracking efficiency to be 66.18% for charged pions at  $p_T$  in (0.05, 0.1) GeV/c.

#### Momentum resolution of charged tracks

The momentum resolution of a charged track is affected by the multiple scattering and the accuracy of the track position from its flight trajectory. The former one is related to

the material, which has a lower atomic number, used by the tracker system. The spatial resolution of the charged track flight trajectory, determined by the accuracy of the track position, is studied for its influence on momentum resolution by applying a set of  $\sigma_{xy}$  from 65 to 130  $\mu\text{m}$  and  $\sigma_z$  from 1240 to 2480  $\mu\text{m}$  proportionally. Because the resolutions of kinematic variable  $\Delta E$  and  $M_{BC}$  are affected by the momentum resolutions of charged tracks, different mass windows are then used to obtain the detection efficiencies of 14 tag modes, which are shown in Fig. 4b. It means that weak dependence from different spatial resolutions is observed. Due to the instability of the ST efficiency, the optimization of momentum resolutions of charged tracks is not changed.

#### Detection efficiency of photons

The energy of photons from  $D_s^-$  decay ranges from less than 0.1 to 1.2 GeV as shown in Fig. 5. The detection efficiency of photons is primarily studied with low energy to be from 50 MeV to 200 MeV. Fig. 4c shows the detection efficiency of 14 tag modes with the variation of detection efficiency, where the optimized point is found to be 88.33% for photons with an average energy of (50, 200) MeV. As for further optimization, the effect on  $\pi$  identification efficiency is quite weak in barrel of the detector, but there is still room for improvement in endcap of the detector.

#### Energy/position resolution of photon

The energy and position resolutions of photons are two primary parameters for photon detection. For 14 tag modes of  $D_s^-$  decay, photon resolutions of photons, i.e. energy ranging from 2.5% to 1.25% and position resolutions ranging 6 mm to 3 mm at 1 GeV, have been tested. It is found that the detection efficiencies of decay modes containing photons are improved, particularly for better energy resolution, as shown in Fig. 4d, e. As a result, photons' energy resolution is set to 1.75%. Moreover, the detection efficiencies of decay modes containing photons are not improved in the optimization of position resolution. As a result, a 6 mm position resolution of photon can satisfy the physics goal of our analysis.

The influence of energy and position resolutions of photons is also studied with the process  $e^+e^- \rightarrow D_s^+ D_s^{*-} + c.c$  at  $\sqrt{s} = 4.18$  GeV, where the energy of photon in  $D_s^{*-} \rightarrow \gamma(\pi^0)D_s^-$  locates within 200 MeV. Two primary parameters of this process are discussed. One is the mass difference of reconstructed  $D_s^{*-}$  and  $D_s^-$ ,  $\Delta M$ , whose resolution is determined by the resolution of photon energy. The other one is the  $\gamma/\pi^0$  contamination in the reconstruction of  $D_s^{*-} \rightarrow \gamma(\pi^0)D_s^-$ . After a series of tests with different energy/position resolutions, it is found that a better energy resolution improves the resolution of  $\Delta M$  as shown in Fig. 6.

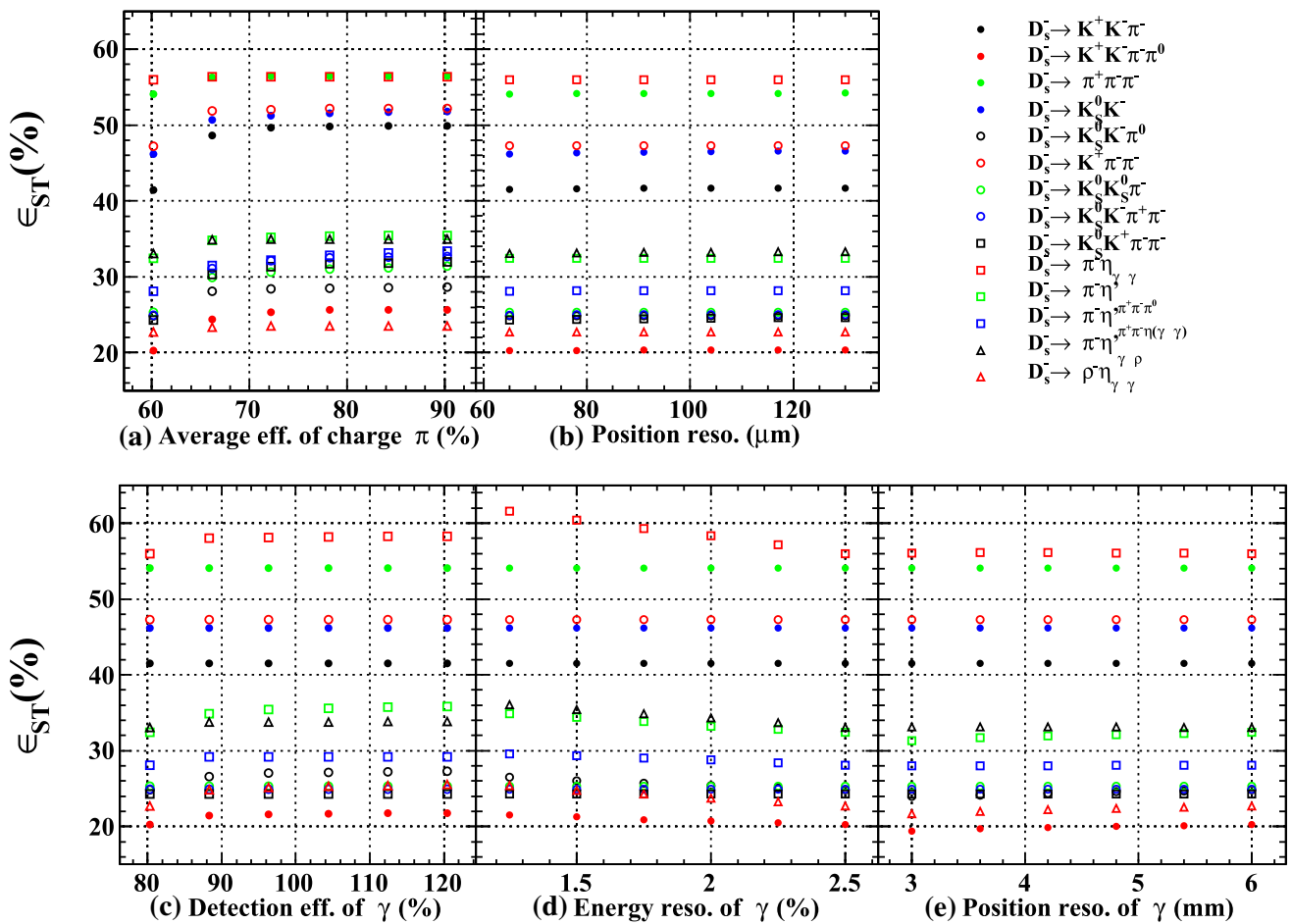


**Fig. 4** The optimization of charged track and photon detection efficiencies and resolutions of 14 tag modes. **a** Shows the average efficiency of charged  $\pi$  in (0.05, 0.1) GeV/c. **b** Shows the Momentum resolution of charged tracks influenced by applying a set of  $\sigma_{xy}$  from 65 to 130  $\mu\text{m}$ .

**c** Shows the detection efficiency of photons in 200 MeV. **d** Shows the energy resolution of photon at 1 GeV. **e** Shows the position resolution of photon at 1 GeV

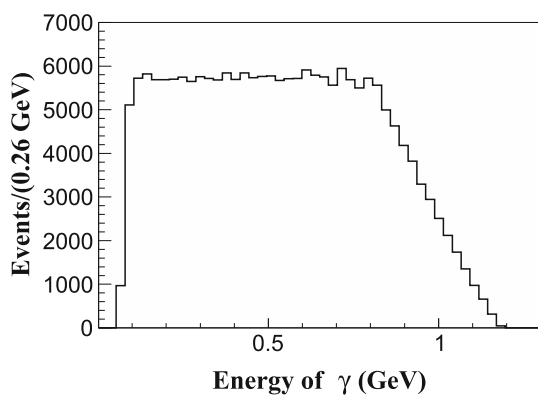


**Fig. 5** The energy of  $\gamma$  from Monte Carlo simulation, which is from  $e^+e^- \rightarrow D_s^+ D_s^-, D_s^+ \rightarrow \mu^+ \nu_\mu, D_s^- \rightarrow \eta \gamma \pi^-$

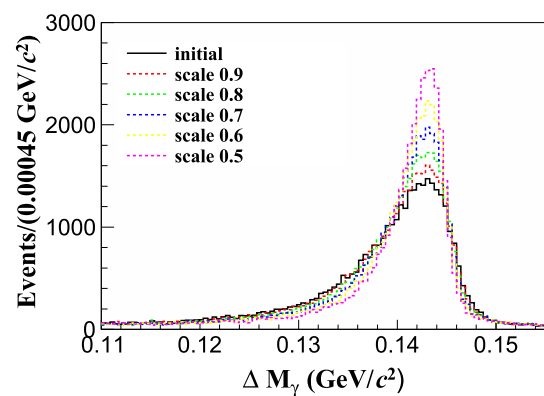


**Fig. 6** The  $\Delta M$  optimization with  $\gamma$  energy resolution. Scale is the optimized proportion of the initial values of detector of response

No obvious improvement is observed for the resolution of  $\Delta M$  in the variation of position resolution, and the  $\pi^0/\gamma$  contamination rate in different energy or position resolutions

of photon remains constant, to be about 28.1%. Although the BF of  $D_s^{*-} \rightarrow \pi^0 D_s^-$  is small, it has an effect to the  $\pi^0/\gamma$  contamination rate and thus the systematic uncertainty.

## $\pi/K$ identification

The identifications of  $\pi$  and  $K$  are essential for the charm physics at STCF. Since the momenta of  $\pi/K$  are relatively low in this analysis, they can be mostly identified by the characteristic ionization energy loss ( $dE/dx$ ) in the tracker system. The simulation indicates that with a  $dE/dx$  resolution of 6%, the  $\pi/K$  can be well separated when  $p < 0.8$  GeV/ $c$ , which can meet the requirement to be 1% for  $\pi/K$  misidentification in this analysis.

## $\mu$ identification

The momentum of  $\mu$  in this analysis is shown in Fig. 3, where the MUD is expected to provide a high identification efficiency for muon and excellent  $\mu/\pi$  mis-identification rate. Ref. [27] describes the details of the baseline design of MUD at STCF. With the performance of MUD provided in Ref. [27], three  $\mu/\pi$  misidentification rates are tested, to be 1%, 1.6% and 3%, corresponding to the identification efficiencies of muon to be 85%, 92% and 97% at  $p_\mu = 1$  GeV/ $c$ . The optimized results is achieved when the  $\mu/\pi$  misidentification rate is 3%.

Based on the discussion above, we use the following detector responses that have been optimized, while others are left alone in the fast simulation. The optimized responses include a good tracking efficiency for low-momentum charged particles, to be averagely around 66.18% in  $p_T \in (0.05, 0.1)$  GeV/ $c$ , a detection efficiency of photons to be averagely around 88.33% for energy within (50, 200) MeV, an energy resolution of photons to be 1.75%, a  $\pi/K$  misidentification rate of 1% at  $p < 0.8$  GeV/ $c$ , a  $\mu/\pi$  misidentification rate of 3% with the MUD performance provided from Ref. [27]. When compared to the default response provided by fast simulation, the detection efficiency for ST is increased by a factor in the range between 1.1 and 1.2, depending on the tag modes, and the efficiency for selecting  $D_s^+ \rightarrow \mu^+ \nu_\mu$  is increased by a factor of 1.3. The change of efficiency can directly indicate the influence of optimization due to the very low background level in the pseudo-data, which is shown as Fig. 2. So Fig. 4 shows the efficiency which can be an indication of figure-of-merit, which means we find the most optimized points to determine the degree of STCF that needs to be optimized in the future instead of endless optimizing to 100%. We feed some pieces of information on optimization back to the Detector R&D. Physicists will research a suitable material, material size, geometry, thickness, *etc* for corresponding sub-detectors to improve the detection efficiency and resolution of particles. There will be some options like a cylindrical  $\mu$ RWELL-based detector and silicon pixel detector that can achieve high tracking efficiency at low energy.

## 5 Results and discussion

With the expected statistical sensitivity of  $\mathcal{B}_{D_s^+ \rightarrow \mu^+ \nu_\mu} = (5.610 \pm 0.017) \times 10^{-3}$  at STCF obtained in this analysis, the world average values of  $G_F$ ,  $m_\mu$ ,  $m_{D_s^+}$  and the lifetime of  $D_s^+$  [3] as listed in Table 2. Therefore, the product value of  $f_{D_s^+} |V_{cs}|$  can be obtained according to Eq. (1)

$$f_{D_s^+} |V_{cs}| = 248.9 \pm 0.4_{\text{stat.}} \text{ MeV.}$$

Taking the CKM matrix element  $|V_{cs}| = 0.97320 \pm 0.00011$  from global fits in the SM [3] or the averaged decay constant  $f_{D_s^+} = 249.9 \pm 0.5$  MeV of recent LQCD calculations [5, 28] as input,  $f_{D_s^+}$  and  $|V_{cs}|$  can be determined separately, to be

$$f_{D_s^+} = 255.8 \pm 0.4_{\text{stat.}} \text{ MeV}$$

and

$$|V_{cs}| = 0.996 \pm 0.002_{\text{stat.}}$$

Combined with the Ref. [29], the systematic uncertainty of the combined  $|V_{cs}|$  and  $f_{D_s^+}$  are estimated to be 0.006 and 1.5, respectively. The relative uncertainty of  $|V_{cs}|$  and  $f_{D_s^+}$  are 0.7% and 0.6%. Here, the systematic uncertainty of  $|V_{cs}|$  comes from the uncertainty of  $\mathcal{B}_{D_s^+ \rightarrow \mu^+ \nu_\mu}$ , the uncertainty of parameters listed in Table 2 and the uncertainty of  $f_{D_s^+}$  from LQCD calculation. Similar for systematic uncertainty of  $f_{D_s^+}$  where the uncertainty from LQCD is replaced by the global fits of  $|V_{cs}|$  in SM. The systematic uncertainties are estimated conservatively and roughly, whose details can be achieved in the future with STCF achievement. Dominant systematic uncertainties are currently contributed by theoretical inputs, FSR, radiative correction. It will be crucial to analyze how the impact of the systematic uncertainties can be reduced at STCF. The accuracy of systematic uncertainty from theoretical calculation should be improved, and the accuracy of systematic uncertainty from the experiment will be studied with real data at STCF in the future.

Besides, the LFU can be tested with the  $\mathcal{B}_{D_s^+ \rightarrow \mu^+ \nu_\mu}$  obtained in this study and the  $\mathcal{B}_{D_s^+ \rightarrow \tau^+ \nu_\tau} = (5.49 \pm$

**Table 2** The values of parameters quoted from PDG [3]

Parameters	Value
$G_F$	$(1.1663787 \pm 0.0000006) \times 10^{-5} \text{ GeV}^2$
$m_\mu$	$105.6583745 \pm 0.0000024 \text{ MeV}/c^2$
$m_{D_s^+}$	$1968.35 \pm 0.07 \text{ MeV}/c^2$
$\tau_{D_s^+}$	$(504 \pm 4) \times 10^{-15} \text{ s}$

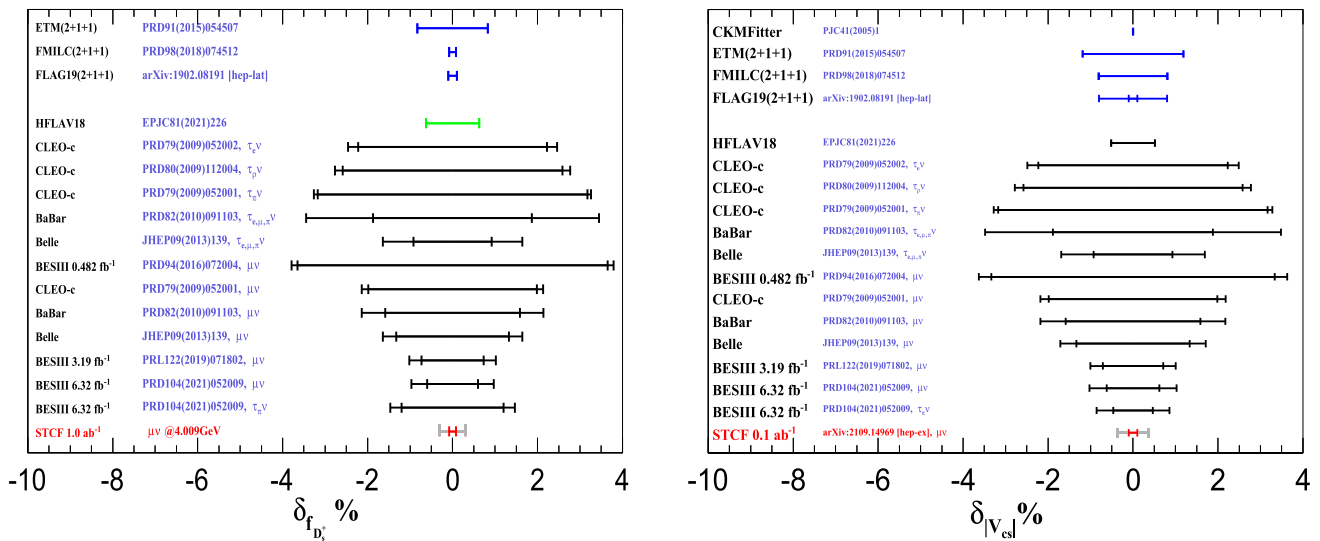


**Fig. 7** The comparisons of  $\delta_{f_{D_s^+}}$  (left) and  $\delta_{|V_{cs}|}$  (right) with previous measurements, the red region represents the statistical uncertainty and the grey are those including systematic uncertainty

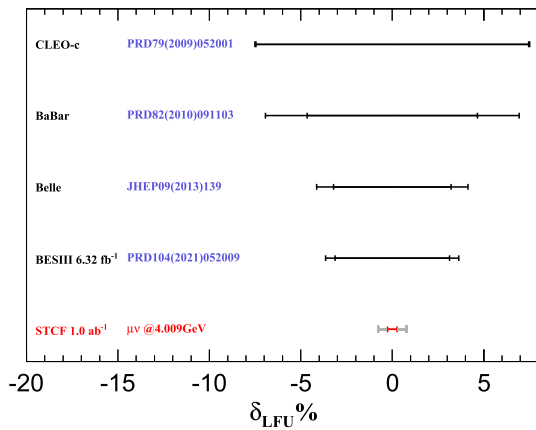


**Fig. 8** The comparison of  $\delta_{LFU}$  with previous measurements, the red region represents the statistics uncertainty and the grey are those including systematic uncertainty

0.02)% [29], to be

$$\frac{\mathcal{B}_{D_s^+ \rightarrow \tau^+ \nu_\tau}}{\mathcal{B}_{D_s^+ \rightarrow \mu^+ \nu_\mu}} = 9.79 \pm 0.05.$$

The systematic uncertainty on the ratio of  $\mathcal{B}_{D_s^+ \rightarrow \tau^+ \nu_\tau}$  to  $\mathcal{B}_{D_s^+ \rightarrow \mu^+ \nu_\mu}$  is estimated to be 1.1%. It is worth mentioning that the  $f_{D_s^+}$  is from recent LQCD calculations and  $|V_{cs}|$  is from the global fits, whose uncertainty will be reduced in the future, therefore the  $f_{D_s^+}$  and  $|V_{cs}|$  determined at STCF will also be improved in the future. As shown in Figs. 7 and 8, the uncertainty of  $f_{D_s^+}$  we determined is less than that from LQCD calculation, requesting an improved LQCD calculation in the future. The expected uncertainty of  $|V_{cs}|$  is close to that from the global fits. The accuracy of the LFU test can

be improved in the experiment, allowing for the search for new physics beyond the SM.

**Acknowledgements** The authors are grateful to the software group of STCF and the physics group of STCF for the profitable discussions. We express our gratitude to the supercomputing center of USTC and Hefei Comprehensive National Science Center for their strong support. This work is supported by the Double First-Class university project foundation of USTC, the Natural Science Foundation of Hunan Province under Contract Nos. 2020RC3054 and 2019JJ30019, and the National Natural Science Foundation of China under Projects Nos. 11625523 and 12122509, and by international partnership program of the Chinese Academy of Sciences Grant No. 211134KYSB20200057.

**Data Availability Statement** The manuscript has associated data in a data repository. [Authors' comment: The data sets generated during and/or analyzed during the current study are available from the corresponding author on reasonable request.]

**Open Access** This article is licensed under a Creative Commons Attribution 4.0 International License, which permits use, sharing, adaptation, distribution and reproduction in any medium or format, as long as you give appropriate credit to the original author(s) and the source, provide a link to the Creative Commons licence, and indicate if changes were made. The images or other third party material in this article are included in the article's Creative Commons licence, unless indicated otherwise in a credit line to the material. If material is not included in the article's Creative Commons licence and your intended use is not permitted by statutory regulation or exceeds the permitted use, you will need to obtain permission directly from the copyright holder. To view a copy of this licence, visit <http://creativecommons.org/licenses/by/4.0/>.  
Funded by SCOAP<sup>3</sup>.

**References**

1. H.P. Peng, High Intensity Electron Positron Accelerator (HIEPA), Super Tau Charm Facility (STCF) in China, talk at Charm2018,

- Novosibirsk, Russia, May 21–25, 2018. Q. Luo, D. Xu, Progress on Preliminary Conceptual study of HIEPA, a super tau-charm factory in China, talk at the 9th International Particle Accelerator Conference (IPAC 2018), held in Vancouver, British Columbia, Canada, April 29–May 4, 2018
2. D. Silverman, H. Yao, *Phys. Rev. D* **38**, 214 (1988). <https://doi.org/10.1103/PhysRevD.38.214>
  3. P.A. Zyla et al. (Particle Data Group), *Prog. Theor. Exp. Phys.* **2020**, 083C01 (2020). <https://doi.org/10.1093/ptep/ptaa104>
  4. A. Bazavov et al., *Phys. Rev. D* **98**, 074512 (2018). <https://doi.org/10.1103/PhysRevD.98.074512>
  5. N. Carrasco et al., *Phys. Rev. D* **91**, 054507 (2015). <https://doi.org/10.1103/PhysRevD.91.054507>
  6. Y.B. Yang et al., *Phys. Rev. D* **92**, 034517 (2015). <https://doi.org/10.1103/PhysRevD.92.517>
  7. Y.S. Amhis et al. (HFLAV), *Eur. Phys. J. C* **81**, 226 (2021). <https://doi.org/10.1140/epjc/s10052-020-8156-7>
  8. M. Ablikim et al. (BESIII), *Phys. Rev. D* **104**, 052009 (2021). <https://doi.org/10.1103/PhysRevD.104.052009>
  9. S. Fajfer, I. Nisandzic, U. Rojec, *Phys. Rev. D* **91**, 094009 (2015). <https://doi.org/10.1103/PhysRevD.91.094009>
  10. G. Branco, P. Ferreira, L. Lavoura, M. Rebelo, M. Sher, J.P. Silva, *Phys. Rep.* **516**, 1 (2012). <https://doi.org/10.1016/j.physrep.2012.02.002>
  11. G. Branco, R. Felipe, F. Joaquim, *Rev. Mod. Phys.* **84**, 515 (2012). <https://doi.org/10.1103/RevModPhys.84.515>
  12. X.-D. Shi, X.-R. Zhou, X.-S. Qin, H.-P. Peng, *JINST* **16**, P03029 (2021). <https://doi.org/10.1088/1748-0221/16/03/P03029>
  13. H. Li, W.H. Huang, D. Liu, Y. Song, M. Shao, X.T. Huang, *JINST* **16**, T04004 (2021). <https://doi.org/10.1088/1748-0221/16/04/T04004>
  14. R.G. Ping, *Chin. Phys. C* **38**, 083001 (2014). <https://doi.org/10.1088/1674-1137/38/8/083001>
  15. E.A. Kuraev, V.S. Fadin, *Sov. J. Nucl. Phys.* **41**, 466 (1985)
  16. E. Barberio, Z. Was, *Comput. Phys. Commun.* **79**, 291 (1994). [https://doi.org/10.1016/0010-4655\(94\)90074-4](https://doi.org/10.1016/0010-4655(94)90074-4)
  17. D.J. Lange, *Nucl. Instrum. Meth. A* **462**, 152 (2001). [https://doi.org/10.1016/S0168-9002\(01\)00089-4](https://doi.org/10.1016/S0168-9002(01)00089-4)
  18. J.C. Chen, G.S. Huang, X.R. Qi, D.H. Zhang, Y.S. Zhu, *Phys. Rev. D* **62**, 034003 (2000). <https://doi.org/10.1103/PhysRevD.62.034003>
  19. H. Albrecht et al. (ARGUS), *Phys. Lett. B* **229**, 304 (1989). [https://doi.org/10.1016/0370-2693\(89\)91177-5](https://doi.org/10.1016/0370-2693(89)91177-5)
  20. M. Ablikim et al. (BESIII), *Phys. Rev. Lett.* **122**, 071802 (2019). <https://doi.org/10.1103/PhysRevLett.122.071802>
  21. M. Ablikim et al. (BESIII), *Phys. Rev. D* **104**, 052009 (2021). <https://doi.org/10.1103/PhysRevD.104.052009>
  22. M. Ablikim et al. (BESIII), *Phys. Rev. Lett.* **127**, 171801 (2021). <https://doi.org/10.1103/PhysRevLett.127.171801>
  23. E. Barberio, Z. Was, *Comput. Phys. Commun.* **79**, 291 (1994). [https://doi.org/10.1016/0010-4655\(94\)90074-4](https://doi.org/10.1016/0010-4655(94)90074-4)
  24. G. Burdman, J.T. Goldman, D. Wyler, *Phys. Rev. D* **51**, 111 (1995). <https://doi.org/10.1103/PhysRevD.51.111>
  25. M. Ablikim et al. (BESIII), *Phys. Rev. D* **89**, 051104 (2014). <https://doi.org/10.1103/PhysRevD.89.051104>
  26. A. Zupanc et al. (Belle), *JHEP* **09**, 139 (2013). [https://doi.org/10.1007/JHEP09\(2013\)139](https://doi.org/10.1007/JHEP09(2013)139)
  27. Z. Fang, Y. Liu, H. Shi, J. Liu, M. Shao, *JINST* **16**, P09022 (2021). <https://doi.org/10.1088/1748-0221/16/09/P09022>
  28. A. Bazavov et al. (Fermilab Lattice, MILC), *Phys. Rev. D* **90**, 074509 (2014). <https://doi.org/10.1103/PhysRevD.90.074509>
  29. H. J. Li, T. Luo, X. Shi, X. Zhou (2021), [arXiv:2110.08864](https://arxiv.org/abs/2110.08864) [hep-ex]